IEEE Robotics and Automation Letters (RA-L) paper, presented at ICRA 2026, Vienna, Austria. Cite as RA-L paper.

Superelastic Tendon-Like Bowden Cables: Advancing Assistive Exoskeletons

Gregorio Pisaneschi, José M. Catalán, Andrea Blanco, Nicola Sancisi, Nicolas García, *Member, IEEE*, and Andrea Zucchelli

***Abstract*—This study introduces a novel Bowden cable (BC) system for hand-assistive exoskeletons employing superelastic (SE) shape memory alloy wires to address key limitations such as efficiency and safety limitations. The unique properties of SE wires enable a single-wire transmission, offering enhanced performance, plus inherent self-sensing and self-limiting capabilities that provide tendon-like overload protection. Experimental results obtained with a setup simulating use conditions demonstrate the superior efficiency of SE wires, with 1/4 the friction of conventional steel cables. In addition, a validated force-sensing capability, achieved by monitoring electrical resistance, proves to accurately detect overloads within 1% force error. This, along with the inherent passive force self-limiting behaviour during simulated collisions, demonstrates the ability of the SE BC to effectively mimic the protective function of biological tendons. Therefore, this biomimetic innovation in soft robotic transmission significantly improves safety and efficiency, presenting a promising advancement for human-robot interaction in assistive and rehabilitative robotics.**

***Index Terms*—Soft robot materials and design, biomimetics, tendon/wire mechanism, safety in HRI.**

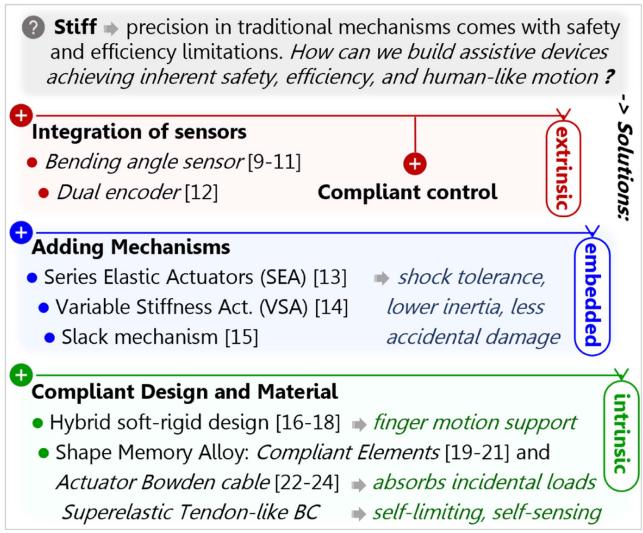

Fig. 1. Emerging trends in soft robotics.

I. Introduction

As THE incidence of hand disabilities resulting from accidents and diseases rises [1], the demand for assistive technologies supporting activities of daily living (ADL) grows. Hand disabilities greatly impact people's independence and quality of life, reducing their ability to carry out ADL. Most hand exoskeletons exist for rehabilitation (e.g., Gloreha [2]), and few are designed for assistance (e.g., Carbonhand [3]). Furthermore, these devices require residual hand movement and are priced at thousands of euros, leaving those with severe disabilities, such as tetraplegia, with no options.

One promising area of research is soft robotics. Its ability to mimic the complex motion of the musculoskeletal system makes it a safer and more adaptable alternative to traditional rigid robotics [4]. For instance, pneumatic hand-assistive exoskeletons (HAEs) offer lightweight and flexible solutions inspired by biological systems [5]. However, they lack the precision of rigid exoskeletons and require bulky external hardware, increasing cost and discomfort [6]. Tendon-sheath actuators (TSAs) are a practical alternative that provides precise control and lightweight design. This enhances wearability and comfort, making TSAs well-suited for HAEs used in ADL [1], [6]. For instance, the Exo-Glove Poli II [7] employs Bowden cables (BCs) to mimic human tendons within a soft structure. However, despite their widespread use, conventional TSAs face challenges, such as frictional losses, inefficient force transmission, and limited durability [8]. In addition, their inherent rigidity may pose safety risks when interacting with the human body [9].

Soft robotics transmissions/actuators try to address these challenges through the main solutions summarised in Fig. 1. The effectiveness of extrinsic solutions depends on the BC model used in the control, and sensor placement can be challenging, affecting force control if placed near the actuator or resulting unpractical if placed near the end-effector [8], [24]. Embedded solutions have drawbacks, such as reduced zero-motion force bandwidth and increased control complexity, which may be acceptable trade-offs [25]. However, variable stiffness actuators (VSAs) and serial elastic actuators (SEAs) often require the

Received 31 March 2025; accepted 3 August 2025. Date of publication 2 September 2025; date of current version 10 September 2025. This article was recommended for publication by Associate Editor Hugo Rodrigue and Editor upon evaluation of the reviewers' comments. *(Corresponding author: Gregorio Pisaneschi.)*

Gregorio Pisaneschi, Nicola Sancisi, and Andrea Zucchelli are with the Department of Industrial Engineering, University of Bologna, 40126 Bologna, Italy (e-mail: gregorio.pisaneschi@unibo.it).

José M. Catalán, Andrea Blanco, and Nicolas García are with the Bioengineering Institute, UMH de Elche, 03202 Elche, Spain.

This article has supplementary downloadable material available at https://doi.org/10.1109/LRA.2025.3605094, provided by the authors.

Digital Object Identifier 10.1109/LRA.2025.3605094

IEEE Robotics and Automation Letters (RA-L) paper, presented at ICRA 2026, Vienna, Austria. Cite as RA-L paper.

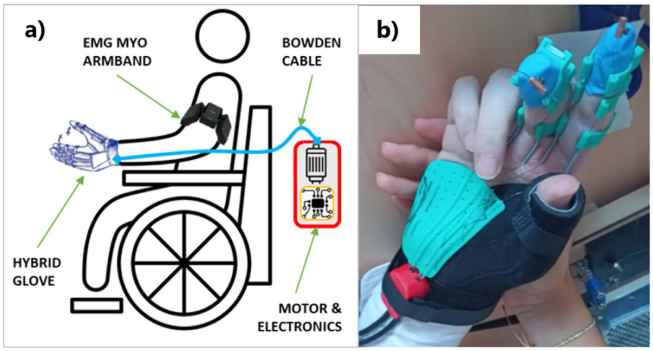

Fig. 2. a) Scheme of the HAE system; b) HAE with SE wires, functional evaluation with one tetraplegic volunteer.

integration of extra bulky and heavy mechanisms, thereby reducing overall wearability. Intrinsic solutions, particularly those using shape memory alloys (SMAs), face limited actuation frequencies and stroke length challenges. Nanomaterials offer another way to realise soft biomimetic actuators [26]; however, current solutions are still being developed and far from being implemented.

In collaboration with the Montecatone Rehabilitation Institute Spinal Unit, this study stems from developing a low-cost, hybrid rigid-soft HAE (Fig. 2) to restore independence in ADL of people with tetraplegia. The HAE features rigid rings interconnected by flexures on the hand back, designed to aid the extension and to guide the flexion performed by a palmar tendon-driven system. Qualitative tests highlighted the limitations of conventional BC. The high friction, in particular, hindered proper gripping. Moreover, potential failures due to cyclic loading, winding curvature and friction (reducing efficiency by up to 90% [27]) compromise robot safety and performance [28]. To address these limitations, we introduce a novel transmission using superelastic (SE) SMA wire within BCs for HAE that can improve efficiency, safety, and durability while minimising additional components. Although superelasticity, allowing large reversible deformation via martensitic transformation (MT), saw successful biomedical use [29], SE BCs remain unexplored; prior works using SE wires only as tendons proved inconclusive, because using a stainless steel (SS) sheath led to premature wire failure [30], [31]. In this study, a PTFE sheath was used, enabling the successful implementation and characterisation of an SE-BC. A custom setup for BC testing was used to compare SE wires and standard SS cables performance under constant load cycling. Furthermore, inspired by the musculoskeletal system, whose Golgi tendon organs provide a protective lengthening reflex [32], this study exploited the MT to mimic this mechanism and tested the electrical resistance variation for overload detection. Thus, the BC test setup was modified for electrical resistance measurement and collision simulation to demonstrate, for the first time, how the inherent force self-limiting mechanism and the electrical resistance self-sensing capability of SE wires can be used synergistically for force feedback control and overload protection in BCs.

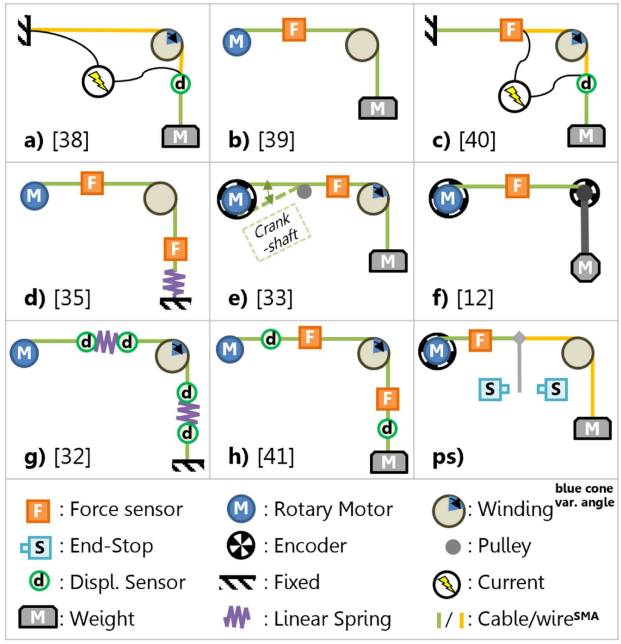

Fig. 3. Setups from literature for testing BCs in order of complexity from a) to h); ps) setup used in the present study.

II. Material and Method

The wire used in this research was a SE Nitinol (55.8% Ni by wt., Ti balanced and Af $-8\,^{\circ}C$) with $0.2\,mm$ diameter (d) and a light oxide surface. The cable used for comparison was a 1x7 strands SS cable with $0.2\,mm$ diameter. The intrinsic flexibility of Nitinol allows it to function in BCs as a single wire. In contrast, the high stiffness of SS requires a multi-strand configuration to provide the necessary flexibility for a BC to bend. The lengths of all the wires and cables used were $150\,mm$. Tensile tests were conducted on SE wires and SS cables on an Instron 5966 universal testing machine with a $10\,kN$ load cell at a constant speed of $50\,mm/min$. SE wires were first cycled 100 times up to 6% of deformation and then returned to a $1\,N$ ($64\,MPa$) load. After the cycling, both the SE wire and the as-received SS cable were subjected to a monotonic traction test until failure.

An overview of the literature was conducted to determine the optimal setup for cyclically stressing wires/cables under various loads, simulating BC operation in HAEs. Fig. 3 presents multiple solutions from the literature, ranging from simple a) to complex h). A common approach across these setups is to use a hanging weight to apply constant force. The setup of Fig. 3(a) [33] tested an actuated SMA and the pulling force T was estimated using capstan's formula:

$$T = We^{\mu\theta} \tag{1}$$

where W is the weight force, μ the kinetic friction and θ the winding angle in radiants. Carlson et al. (Fig. 3(b) [34]) used a load cell to determine the cable efficiency (W/T) under quasi-static conditions, validating the use of (1) to winded BCs. Villoslada et al. tested actuated SMA BCs measuring both force and displacement (Fig. 3(c) [35]). In et al. tested SE wire with a U-shaped metal sheath (Fig. 3(d) [30]), estimating friction.

IEEE Robotics and Automation Letters (RA-L) paper, presented at ICRA 2026, Vienna, Austria. Cite as RA-L paper.

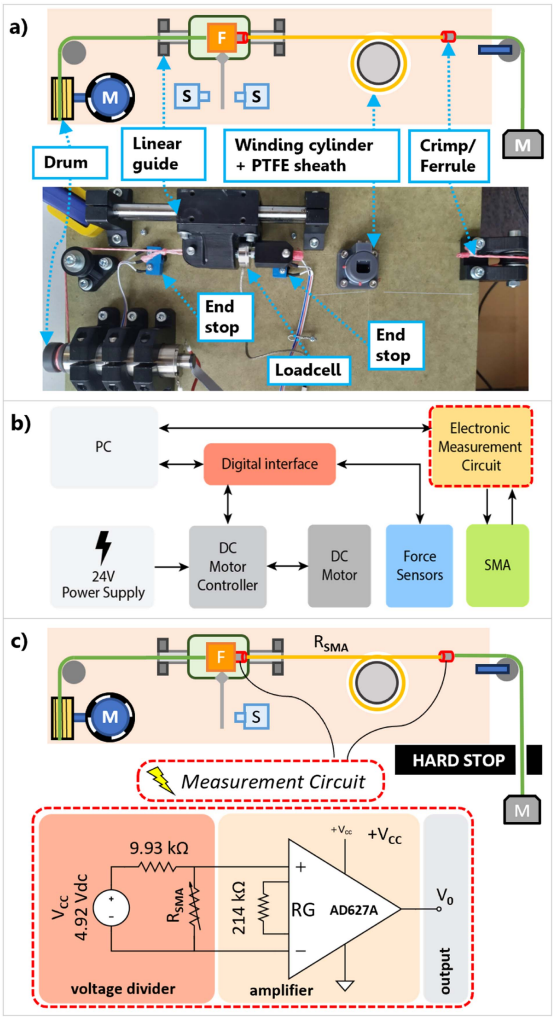

Fig. 4. a) setup for SE and SS efficiency tests, b) scheme of the connections, c) modified setup for SE self-sensing tests.

Jeong et al. conducted a comprehensive study on the reliability and durability of BCs (Fig. 3(e) [28]). Yin et al. validated collision detection in a rotative joint with an encoder (Fig. 3(g) [11]). Chen et al. setup (Fig. 3(g) [27]) was used for characterising friction in small-scale BC. Goiriena et al. (Fig. 3(h) [36]) evaluated both the force and displacement transmission efficiencies. While simpler setups such as $a), b)$ are limited to quasi-static testing for material comparison and fatigue analysis, more complex setups such as $g), h)$ enable dynamic characterisation. In this study, a compromise between these solutions was chosen (Fig. $3ps$) capable of replicating the real-world bending stress and cyclic loading conditions of an HAE BC while measuring efficiency and friction minimising the setup complexity.

The setup used in the present study is detailed in Fig. 4(a) with a schematic of the connection shown in Fig. 4(b). It consisted of a drum mounted on a MAXON DCX 22L 12V motor with a 21:1 planetary gear and an encoder. The motor was controlled by a Maxon Escon 36/2 DC driver for speed control. A Phidget InterfaceKit was used as a digital input/output interface, and a Phidget Bridge was used for load cell and SE wire voltage measurement. The load cell (OMEGA LCM201-100N) was calibrated and had

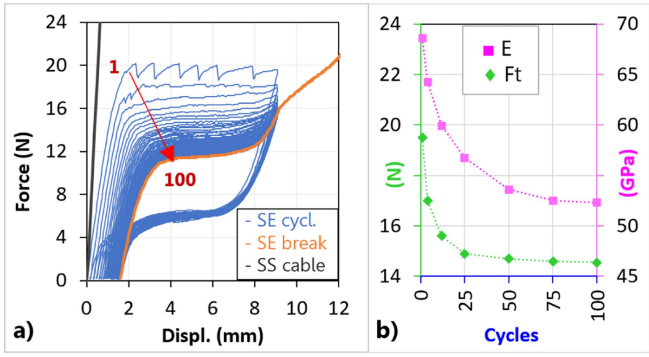

Fig. 5. a) Tensile test of SE wire and SS cable. b) Young's modulus and transformational force over cycles of SE wire.

a linearity accuracy of $\pm 1.0\%$ of full-scale. A PC was used for data logging and control. To mimic a BC, a PTFE sleeve ($0.7\ mm$ inner diameter, $0.25\ mm$ wall thickness) was wrapped 360° around a cylinder of $20\ mm$ diameter ($D/d = 100$ [37]). Two end-stops, snap-action switches, triggered the motor reversal for cycling, allowing a stroke of $54\ mm$.

A. Mechanical Efficiency Tests Method

For each test, a new SE and SS cable and PTFE sleeve were installed Fig. 4(a). Three load conditions were tested using weights of $0.5\ kg$, $1.0\ kg$, and $1.5\ kg$, denoted here as load case "05", "10", and "15". Three tests were conducted for each material and load condition. Each test consisted of 100 load cycles performed at a constant speed of $10\ mm/s$ (equal to that required by the HAE). The motor controller was configured with acceleration ramps of $0.04\ sec$ to avoid stressing the BC or pushing the end-stop. The direction of motion was automatically reversed when the mechanism triggered the end-stops. A Python script controlled the system and recorded force data at a $100\ Hz$ sampling frequency. The raw signal was processed with a Butterworth low-pass filter at a $2Hz$ cutoff to reduce noise. For each cycle, transmission efficiency was calculated as the ratio of the weight force (W) to the average measured pulling force (T). The kinetic friction was subsequently calculated using (1).

B. Electro-Mechanical Testing Method

To validate the SE wire's self-sensing capabilities, the experimental setup was modified. An electronic measurement circuit (Fig. 4(c) measured the voltage drop across the SE wire ($2.2\ mV$ to $5\ mV$). To ensure a stable connection, the circuit leads were welded to the wire's crimps. In the preliminary experiment, a procedure was performed to correlate resistance to force. A $1.0\ kg$ weight was lifted until blocked by a hard stop, simulating a collision. The force sensor's reading was monitored, and the motor direction was reversed when the force exceeded a $19\ N$ threshold. The wire's electrical resistance was recorded simultaneously throughout this process to establish a clear force-resistance relationship (8(b)). In the validation experiment, a resistance threshold corresponding to the desired force limit was set. th a simple control: the resistance from the

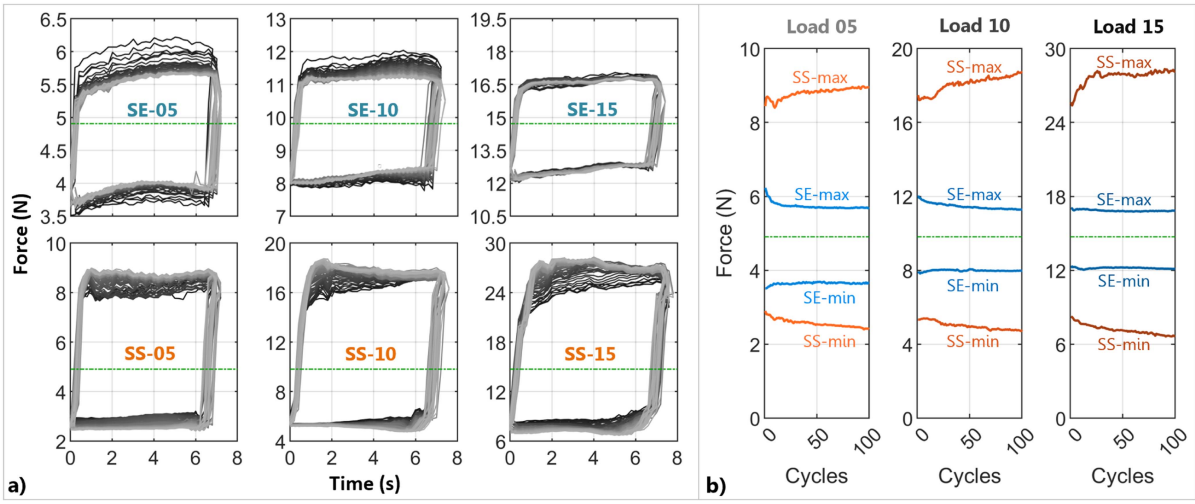

Fig. 6. Results of cyclic testing of SS cable and SE wire. a) force vs time for all cycles (the higher the cycle number, the lighter the line colour). b) maximum and minimum force over cycles. The green dotted line represents the weight force.

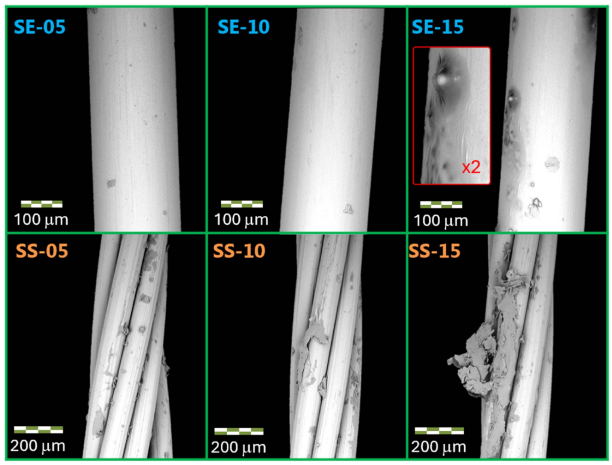

Fig. 7. Micrographs of SS cables and SE wires after cycling.

measurement circuit was continuously monitored, and when the value exceeded the set threshold, a command to reverse the motor direction was sent. The resulting force was recorded throughout this process to assess the accuracy of this proof-of-concept overload detection method.

III. Results and Discussion

Fig. 5(a) shows the SE wire's tensile test result. In the first cycle (1), nucleation of stress-induced martensite bands associated with the force drop can be observed [38]. After 100 cycles, the mechanical response stabilised: in Fig. 5(b) it can be observed that both Young's modulus (E) and the transformation force measured @6 mm (Ft) decreased progressively due to the training effect [38]. Final values of E and Ft are $52\,GPa$ and $13\,N$ ($405\,MPa$). The ultimate tensile strength was $38,5\,N$ ($1235\,MPa$) at $19.5\,mm$ (13% deformation). The SS cable tensile test (black line in Fig. 5(a)) results showed a stiffer behaviour with a tensile force at break of $85\,N$, with a displacement of $3\,mm$.

TABLE I
SS Cables and SE Wire Cycling Test Results

Tests series	Efficiency (%)	Friction (μ)	Work trendline[a] (mJ)
SE-05	86.6 ± 4.6	0.0100 ± 0.0036	$132 - 0.19x$
SE-10	87.0 ± 0.9	0.0096 ± 0.0007	$234 - 0.35x$
SE-15	88.0 ± 1.4	0.0089 ± 0.0011	$299 - 0.03x$
SS-05	54.9 ± 0.3	0.0415 ± 0.0003	$339 + 0.73x$
SS-10	54.7 ± 1.1	0.0417 ± 0.0013	$727 + 1.20x$
SS-15	51.8 ± 0.7	0.0455 ± 0.0010	$1182 + 1.81x$

[a] Trendline equation of force-time cycles area (Fig.6a) multiplied by the constant speed, over cycles (x is the number of cycles).

A. Mechanical Efficiency Tests Results and Discussion

Fig. 6(a) presents force-time graphs from one of the cycling tests for each load case. Each cycle was obtained by inverting the time as the motor reverses direction, with overlapping lines representing successive cycles (the higher the cycle number, the lighter the line colour). The SE performed better than the SS in each load case, exhibiting lower pulling forces and smaller hysteresis. The SE performance improved over the cycles and with higher loads, whereas the opposite occurred for SS. Specifically, in the SE experiments, the pulling force was lower at the beginning of the cycle and progressively increased. Additionally, it decreased with cycling for SE-05 and SE-10, whereas it remained stable for SE-15. In contrast, the pulling force increased over the cycles for the SS experiments, with a more significant growth in the initial force observed for SS-10 and SS-15.

In Table I, the average values over cycling of efficiency and friction during pulling, from equation (1), are reported. The SE wire demonstrated higher efficiency and lower friction across all experiments. In addition, in Tab.I the trendline of the work over the cycle is reported, showing lower values with decreasing trends for the SE in contrast to the higher values and the increasing trend of SS. Fig. 7 shows SEM images of the SS cable and SE wires after 100 cycles for all load cases. It can be observed that the SE wires remained clean in the 05 and 10 load cases.

IEEE Robotics and Automation Letters (RA-L) paper, presented at ICRA 2026, Vienna, Austria. Cite as RA-L paper.

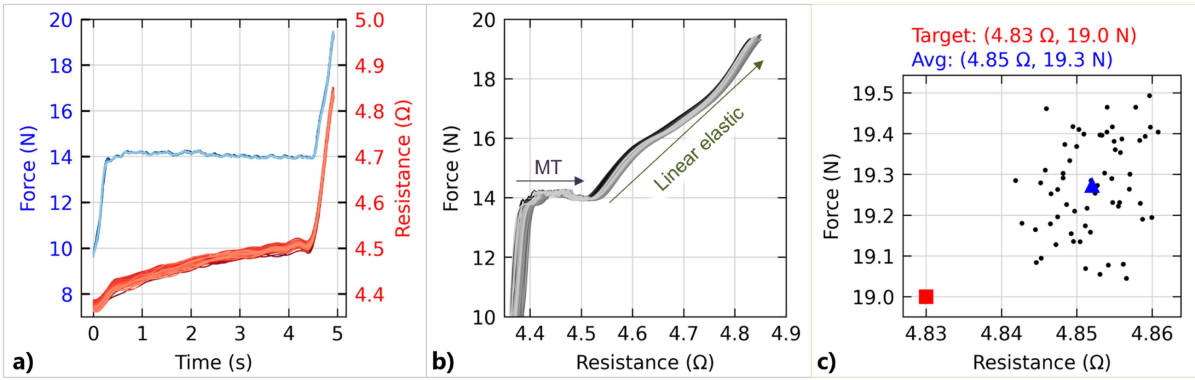

Fig. 8. Results from the experiment with force threshold: a) force and electrical resistance over time, b) force vs resistance. Results from the experiment with resistance threshold: c) values at motor inversion after reaching the threshold (black dots).

In load case 15, partial adhesion of PTFE and the appearance of wrinkles, possibly caused by high deformation, can be observed. The adhered PTFE could explain the slight decrease in friction for SE-15. In contrast, the SS cable exhibited an increasing accumulation of PTFE debris with higher loads. This is likely due to strand-induced abrasion and twisting of the cable, which intensified with greater hysteresis, resulting in increased SS cable friction that can lead to PTFE tube delamination [7].

The present study found a ten-fold lower friction for an SE wire with a PTFE sheath versus a metal one [30], consistent with the known friction reduction provided by PTFE housing compared to metal [34]. Moreover, although lower stiffness typically increases friction [27], the less rigid SE wires prove more efficient than SS wires due to their smoother surfaces. Finally, although low-friction polymer coatings can reduce friction of SS cables by 40% [34], it would still be higher than that of SE wires, and the durability of the coatings is uncertain. Interestingly, higher loads seem to improve the efficiency of SE wires in BCs.

B. Electro-Mechanical Tests Results and Discussion

Fig. 8(a), (b) present results from cyclic pulling tests performed using force threshold control, with cycle progression indicated by the progressively lighter line shading. Fig. 8(a), which plots force and electrical resistance against time, effectively demonstrates the system's self-limiting behaviour upon impacting the hard stop. After an initial rapid rise, the force distinctly plateaus near $14\ N$ for a significant duration of time. During this plateau phase, the resistance increases linearly due to the wire stretching [39]. After this plateau, the force shows a linear increase, exceeding the $19\ N$ experimental threshold (delay probably caused by inertia and control system promptness), which is accompanied by a concurrent and steeper linear rise in resistance. The force-resistance relationship (Fig. 8(b)) clearly shows two distinct operational regimes after the initial contact, highlighting the potential for using resistance measurements to infer force levels during and after MT in BC. Fig. 8(c) presents the experiment's results with the resistance threshold $4.83\ \Omega$ (corresponding to $19\ N$). It reports the force and resistance values recorded at motor reversal, along with the target value (red square) and the average of these measured endpoints (blue triangle). These endpoints exhibit high precision, clustering around the average value with a standard deviation of $0.005\ \Omega$ for resistance and $0.118\ N$ for force. Accuracy is also good, indicated by the minor offset between the average endpoint and the target: $+0.022\ \Omega$ higher in resistance and $+0.27\ N$ higher in force, potentially due to the system lag effects observed previously. The combination of high precision and accuracy demonstrates that the resistance threshold provides an effective and reliable method for overload detection.

IV. Findings

Efficiency. The high strength and flexibility of SE wires enable a single-wire configuration with a smoother surface, resulting in significantly lower friction and nearly double the efficiency compared to SS cables, whose multi-strand leads to high friction and sheath wear [7]. The use of SE BCs could result in more efficient assistive devices that require less energy to operate.

Self-Sensing. Electrical resistance measurements in SE wires can be used for strain sensing [40] and, as demonstrated in this study, to detect MTs and overloads with less than 1% of error of full scale. This inherent self-sensing capability eliminates the need for external sensors, simplifying the design and reducing the bulk of soft, wearable structures.

Safety. SE wires' inherent self-limiting force behaviour provides a crucial safety mechanism. Upon reaching a certain force threshold, the force plateaus, and an abrupt change in resistance occurs. This phenomenon can trigger deactivation, rapidly reducing the force to a safer level and preventing potential damage or injury.

Applicability. The SE BC was integrated into the HAE prototype as a mechanical component for preliminary tests in-lab (supplementary video) and with one tetraplegic volunteer (Fig. 2(b)). In these qualitative assessments, the SE BC enabled more effective gripping compared to the SS cable. However, clinical trials with quantitative metrics are required for a full validation of the HAE full functionality.

V. Conclusion

This study provides compelling evidence for the significant advantages of using superelastic (SE) Nitinol wires in Bowden cable (BC) assistive devices. By outperforming

traditional stainless-steel cables in efficiency and friction reduction, SE wires enable the development of more responsive and energy-efficient systems. Furthermore, the study successfully demonstrated the use of electrical resistance changes in SE wires for self-sensing, enabling the detection of collisions and eliminating the need for external sensors. Finally, by mimicking the protective functions of the human tendon, SE wires' inherent self-limiting force behaviour can contribute to creating more compliant and safe exoskeletons. Integrating SE BCs can revolutionise assistive devices, improving the quality of life and independence for individuals with disabilities. While this study validates the self-limiting concept under controlled, quasi-static conditions, future work must test the system's effectiveness and response time in more dynamic, unpredictable scenarios, such as abrupt impacts, to fully assess its potential for creating safer assistive devices.

REFERENCES

[1] T. D. Plessis, K. Djouani, and C. Oosthuizen, "A review of active hand exoskeletons for rehabilitation and assistance," *Robotics*, vol. 10, no. 1, Mar. 2021, Art. no. 40.

[2] A. Borboni, M. Mor, and R. Faglia, "Gloreha-hand robotic rehabilitation: Design, mechanical model, and experiments," *J. Dyn. Syst. Meas. Control*, vol. 138, no. 11, Nov. 2016, Art. no. 111003.

[3] M. Nilsson, J. Ingvast, J. Wikander, and H. V. Holst, "The soft extra muscle system for improving the grasping capability in neurological rehabilitation," in *Proc. IEEE-EMBS Conf. Biomed. Eng. Sci.*, 2012, pp. 412–417.

[4] C.-Y. Chu and R. M. Patterson, "Soft robotic devices for hand rehabilitation and assistance: A narrative review," *J. Neuroeng. Rehabil.*, vol. 15, no. 1, Dec. 2018, Art. no. 9.

[5] L. Cappello et al., "Assisting hand function after spinal cord injury with a fabric-based soft robotic glove," *J. Neuroeng. Rehabil.*, vol. 15, no. 1, Dec. 2018, Art. no. 59.

[6] G. M. Achilli et al., "Soft, rigid, and hybrid robotic exoskeletons for hand rehabilitation: Roadmap with impairment-oriented rationale for devices design and selection," *Appl. Sci.*, vol. 13, no. 20, Oct. 2023, Art. no. 11287.

[7] B. B. Kang et al., "Exo-glove poly II: A polymer-based soft wearable robot for the hand with a tendon-driven actuation system," *Soft Robot.*, vol. 6, no. 2, pp. 214–227, Apr. 2019.

[8] U. Jeong and K.-J. Cho, "Control of a bowden-cable actuation system with embedded BoASensor for soft wearable robots," *IEEE Trans. Ind. Electron.*, vol. 67, no. 9, pp. 7669–7680, Sep. 2020.

[9] U. A. T. Hofmann, T. Bützer, O. Lambercy, and R. Gassert, "Design and evaluation of a Bowden-cable-based remote actuation system for wearable robotics," *IEEE Robot. Autom. Lett.*, vol. 3, no. 3, pp. 2101–2108, Jul. 2018.

[10] S.-H. Kim, U. Jeong, and K.-J. Cho, "Multiparameter remote contact force sensor with embedded bend sensing for tendon-driven hand robots," *IEEE/ASME Trans. Mechatron.*, vol. 29, no. 1, pp. 557–566, Feb. 2024.

[11] M. Yin, H. Wu, Z. Xu, W. Han, and Z. Zhao, "Compliant control of single tendon-sheath actuators applied to a robotic manipulator," *IEEE Access*, vol. 8, pp. 37361–37371, 2020.

[12] L. Ai et al., "Design and control of a cable-driven series elastic actuator for exoskeleton," in *Proc. IEEE 4th Int. Conf. Intell. Auton. Syst.*, 2021, pp. 335–339.

[13] H. Choi, K. B. Kim, S. Cheon, J. -H. Shin, and K. -J. Cho, "Soft robotic glove modulating joint torque through novel passive extensor mechanisms," *IEEE Robot. Autom. Lett.*, vol. 9, no. 4, pp. 3227–3234, Apr. 2024.

[14] H. In, U. Jeong, H. Lee, and K. -J. Cho, "A novel slack-enabling tendon drive that improves efficiency, size, and safety in soft wearable robots," *IEEE/ASME Trans. Mechatron.*, vol. 22, no. 1, pp. 59–70, Feb. 2017.

[15] C. J. W. Haarman, E. E. G. Hekman, J. S. Rietman, and H. V. D. Kooij, "Mechanical design and feasibility of a finger exoskeleton to support finger extension of severely affected stroke patients," *IEEE Trans. Neural Syst. Rehabil. Eng.*, vol. 31, pp. 1268–1276, 2023.

[16] J. Arata, K. Ohmoto, R. Gassert, O. Lambercy, H. Fujimoto, and I. Wada, "A new hand exoskeleton device for rehabilitation using a three-layered sliding spring mechanism," in *Proc. IEEE Int. Conf. Robot. Automat.*, 2013, pp. 3902–3907.

[17] T. Bützer et al., "Fully wearable actuated soft exoskeleton for grasping assistance in everyday activities," *Soft Robot.*, vol. 8, no. 2, pp. 128–143, Apr. 2021.

[18] S. Pittaccio et al., "Implementation, testing and pilot clinical evaluation of superelastic splints that decrease joint stiffness," *Ann. Biomed. Eng.*, vol. 41, no. 9, pp. 2003–2017, Sep. 2013.

[19] L. Deberg et al., "An SMA passive ankle foot orthosis: Design, modeling, and experimental evaluation," *Smart Mater. Res.*, vol. 2014, pp. 1–11, Jun. 2014.

[20] F. Sadeghian et al., "Compliant orthoses for repositioning of knee joint based on super-elasticity of shape memory alloys," *J. Intell. Mater. Syst. Struct.*, vol. 29, no. 15, pp. 3136–3150, Sep. 2018.

[21] A. Villoslada, A. Flores-Caballero, D. Copaci, D. Blanco, and L. Moreno, "High-displacement fast-cooling flexible shape memory alloy actuator: Application to an anthropomorphic robotic hand," in *Proc. IEEE-RAS Int. Conf. Humanoid Robots*, 2014, pp. 27–32.

[22] D. Serrano, D. Copaci, J. Arias, L. E. Moreno, and D. Blanco, "SMA-based soft exo-glove," *IEEE Robot. Autom. Lett.*, vol. 8, no. 9, pp. 5448–5455, Sep. 2023.

[23] D. Copaci, D. S. D. Cerro, J. A. Guadalupe, L. M. Lorente, and D. B. Rojas, "sEMG-Controlled soft exo-glove for assistive rehabilitation therapies," *IEEE Access*, vol. 12, pp. 43506–43518, 2024.

[24] U. Jeong and K.-J. Cho, "A feasibility study on tension control of bowden-cable based on a dual-wire scheme," in *Proc. IEEE Int. Conf. Robot. Automat.*, 2017, pp. 3690–3695.

[25] H. Vallery, J. Veneman, E. V. Asseldonk, R. Ekkelenkamp, M. Buss, and H. V. D. Kooij, "Compliant actuation of rehabilitation robots," *IEEE Robot. Autom. Mag.*, vol. 15, no. 3, pp. 60–69, Sep. 2008.

[26] C. Gotti et al., "Biomimetic hierarchically arranged nanofibrous structures resembling the architecture and the passive mechanical properties of skeletal muscles: A step forward toward artificial muscle," *Front. Bioeng. Biotechnol.*, vol. 8, Jul. 2020, Art. no. 767.

[27] D. Chen, Y. Yun, and A. D. Deshpande, "Experimental characterization of bowden cable friction," in *Proc. IEEE Int. Conf. Robot. Automat.*, 2014, pp. 5927–5933.

[28] U. Jeong et al., "Reliability analysis of a tendon-driven actuation for soft robots," *Int. J. Robot. Res.*, vol. 40, no. 1, pp. 494–511, Jan. 2021.

[29] T. Duerig, A. Pelton, and D. Stöckel, "An overview of nitinol medical applications," *Mater. Sci. Eng. A*, vol. 273–275, pp. 149–160, Dec. 1999.

[30] H. In, D. Lee, and K.-J. Cho, "Investigation of friction characteristics of a tendon driven wearable robotic hand," in *Proc. Int. Conf. Control, Automat. Syst.*, 2010, pp. 568–573.

[31] HyunKi In et al., "Jointless structure and under-actuation mechanism for compact hand exoskeleton," in *Proc. IEEE Int. Conf. Rehabil. Robot.*, 2011, pp. 1–6.

[32] J. Hall and G. Arthur, *Motor Functions of the Spinal Cord; the Cord Reflexes*, 11st ed. Amsterdam, The Netherlands: Elsevier Saunders, 2006, pp. 673–684.

[33] J. Leng et al., "Design of a novel flexible shape memory alloy actuator with multilayer tubular structure for easy integration into a confined space," *Smart Mater. Struct.*, vol. 25, no. 2, Feb. 2016, Art. no. 025007.

[34] L. E. Carlson, B. D. Veatch, and D. D. Frey, "Efficiency of prosthetic cable and housing," *J. Prosthetics Orthotics*, vol. 7, no. 3, pp. 96–99, 1995.

[35] Á. Villoslada, "Design of a shape memory alloy actuator for soft wearable robots," Doctoral dissertation, Universidad Carlos III de Madrid, Madrid, Spain, 2019.

[36] A. Goiriena, I. Retolaza, A. Cenitagoya, F. Martinez, S. Riano, and J. Landaluze, "Analysis of bowden cable transmission performance for orthosis applications," in *Proc. IEEE Int. Conf. Mechatron.*, 2009, pp. 1–6.

[37] G. Rebel and R. Verreet, "Radial pressure damage analysis of wire ropes operating on multi-layer drum winders," in *Proc. Hoist Haul 2010 Conf., Soc. Mining, Metall., Exploration*, Las Vegas, USA, 2010, pp. 317–327.

[38] N. Zotov et al., "Change of transformation mechanism during pseudoelastic cycling of NiTi shape memory alloys," *Mater. Sci. Eng. A*, vol. 682, pp. 178–191, Jan. 2017.

[39] J. Ferčec, I. Anžel, and R. Rudolf, "Stress dependent electrical resistivity of orthodontic wire from the shape memory alloy NiTi," *Mater. Des.*, vol. 55, pp. 699–706, Mar. 2014.

[40] X. Wu, Y. Fan, and J. Wu, "A study on the variations of the electrical resistance for NiTi shape memory alloy wires during the thermo-mechanical loading," *Mater. Des.*, vol. 21, no. 6, pp. 511–515, Dec. 2000.